ChemComm

FEATURE ARTICLE

Cite this: *Chem. Commun.*, 2022, **58**, 4931

Understanding the reactivity of frustrated Lewis pairs with the help of the activation strain model–energy decomposition analysis method

Israel Fernández

Received 13th January 2022,
Accepted 21st March 2022

DOI: 10.1039/d2cc00233g

rsc.li/chemcomm

This Feature article presents recent representative applications of the combination of the Activation Strain Model of reactivity and the Energy Decomposition Analysis methods to understand the reactivity of Frustrated Lewis Pairs (FLPs). This approach has been helpful to not only gain a deeper quantitative insight into the factors controlling the cooperative action between the Lewis acid/base partners but also to rationally design highly active systems for different bond activation reactions. Issues such as the influence of the nature of the FLP antagonists or the substituents directly attached to them on the reactivity are covered herein, which are crucial for the future development of this fascinating family of compounds.

1. Introduction

The term Frustrated Lewis pairs (FLPs) refers to species typically composed of a pair of a sterically encumbered Lewis acid (LA) and Lewis base (LB), where the formation of a classical donor–acceptor bond between both centers is severely hampered.[1,2] As a consequence, these compounds exhibit a rather peculiar bonding situation which is reflected in a unique and rich reactivity deriving from the cooperative action of the FLP antagonists.[2] Indeed, since the seminal report by Stephan and co-workers on the metal-free and reversible activation of H_2 by the $(C_6H_2Me_3)_2P–(C_6F_4)–B(C_6F_5)_2$ FLP,[3] a good number of different small molecule activation reactions (CO, CO_2, N_2O, SO_2, *etc.*) have been achieved. In addition, FLPs are also able to promote other interesting processes spanning from hydrogenations of unsaturated compounds even in an asymmetric manner[4] to polymerization reactions[5] or heterogeneous catalysis,[6] which illustrates the great usefulness of this family of compounds. In parallel, an impressive number of highly active, either inter- or intramolecular, FLPs have been developed, expanding the traditional group 13/group 15 combinations to systems having transition metal fragments in their structures.[7]

The significant development of the chemistry of FLPs in recent years has been accompanied by studies devoted to rationalizing the reaction mechanisms involved in the above commented FLP-mediated transformations. In particular, for the parent H_2 activation reaction, which is considered as the most representative transformation in the FLP chemistry,[4] two plausible reactivity models have been proposed, namely: (a) the electron transfer (ET) model, proposed by Pápai and co-workers in analogy with the transition metal-mediated H_2 activation,[8] and (b) the electric field (EF) model, suggested by Grimme and co-workers.[9] While the ET model is based on cooperative orbital interactions leading to an electronic density flow from the Lewis base lone pair to the $\sigma^*(H_2)$ molecular orbital and from $\sigma(H_2)$ to the empty orbital on the Lewis acidic center, the EF model establishes that the H_2 molecule becomes polarized

Departamento de Química Orgánica I and Centro de Innovación en Química Avanzada (ORFEO-CINQA), Facultad de Ciencias Químicas, Universidad Complutense de Madrid, 28040-Madrid, Spain. E-mail: israel@quim.ucm.es

Israel Fernández

Israel Fernández (Madrid, 1977) studied Chemistry at the Universidad Complutense de Madrid (UCM) and obtained his doctoral degree in 2005 (with honors) from the same university. After a postdoctoral stay at the Philipps-Universität Marburg under the supervision of Prof. G. Frenking, he returned to the UCM where he is currently "Profesor Titular". IF has received several awards including the Young-Researcher Award from the Spanish Royal Society of Chemistry and the Barluenga Medal. His current research interests comprise the application of state-of-the-art computational methods to quantitatively understand the bonding situation and reactivity of organic and organometallic compounds.

within the cavity created by the presence of bulky groups attached to the donor/acceptor sites, inducing an almost barrierless bond splitting as a consequence of the existence of electric fields. Although both models are conceptually rather different, they share a common feature, namely the formation of an initial pre-organized or encounter complex Lewis pair, which has been identified experimentally,[10] and where dispersion interactions play a key role. Recent research has also widened these traditional two-electron mechanisms to single-electron, radical mechanisms,[11] which have led to new reactivity modes.

Despite the significance and applicability of the above models, a more quantitative understanding of the cooperative action of the FLP antagonists during the activation reaction is lacking. This more detailed understanding is crucial to allow a rational design of either more active FLP systems or even new transformations. In this sense, over the recent years, we have successfully developed a different computational approach based on the combination of the so-called Activation Strain Model (ASM) of reactivity[12] and the Energy Decomposition Analysis (EDA)[13] method, which has proven to provide a deeper and quantitative insight into those physical factors controlling fundamental reactions in organic,[14] organometallic and main-group chemistry.[15] In this Feature article, we summarize our recent efforts to understand in detail the reactivity of FLPs by showing representative applications of the ASM–EDA method to different processes mediated by these fascinating species.

2. The combined activation strain model and energy decomposition analysis approach

As this computational approach has been the focus of recent review articles,[12] herein we only briefly summarize the basics of this methodology.

The ASM is a systematic development of the Energy Decomposition Analysis (EDA)[13] method (see below) proposed by Morokuma[16] and Ziegler and Rauk[17] to understand the nature of the chemical bonding in stable molecules. Within the ASM, the height of reaction barriers is described and understood in terms of the original reactants. Thus, the potential energy surface $\Delta E(\zeta)$ is decomposed, along the reaction coordinate ζ, into the strain ($\Delta E_{\text{strain}}(\zeta)$) that derives from the distortion of the individual reactants from their initial equilibrium geometries plus the actual interaction $\Delta E_{\text{int}}(\zeta)$ between the increasingly deformed reactants along the reaction coordinate (eqn (1)):

$$\Delta E(\zeta) = \Delta E_{\text{strain}}(\zeta) + \Delta E_{\text{int}}(\zeta) \quad (1)$$

It is the interplay between $\Delta E_{\text{strain}}(\zeta)$ and $\Delta E_{\text{int}}(\zeta)$ that determines if and at which point along ζ a barrier arises, namely, at the point where $d\Delta E_{\text{strain}}(\zeta)/d\zeta = -d\Delta E_{\text{int}}(\zeta)/d\zeta$ is satisfied.

The ASM method can be combined with the EDA method to quantitatively partition the $\Delta E_{\text{int}}(\zeta)$ term. Within this approach, the total interaction between the reactants is further decomposed into the following chemically meaningful terms (eqn (2)):

$$\Delta E_{\text{int}}(\zeta) = \Delta V_{\text{elstat}}(\zeta) + \Delta E_{\text{Pauli}}(\zeta) + \Delta E_{\text{orb}}(\zeta) + \Delta E_{\text{disp}}(\zeta) \quad (2)$$

where the term ΔV_{elstat} stands for the classical electrostatic interaction between the unperturbed charge distributions of the deformed reactants and is usually attractive. The Pauli repulsion ΔE_{Pauli} comprises the destabilizing interactions between occupied orbitals and is responsible for any steric repulsion. The orbital interaction ΔE_{orb} accounts for charge transfer (interaction between occupied orbitals on one moiety with unoccupied orbitals on the other, including HOMO–LUMO interactions) and polarization (empty-occupied orbital mixing on one fragment due to the presence of another fragment). Finally, the ΔE_{disp} term takes into account the interactions resulting from dispersion forces.

Moreover, the NOCV (Natural Orbital for Chemical Valence)[18] extension of the EDA method can be also used to further partition the ΔE_{orb} term. The EDA–NOCV approach provides pairwise energy contributions for each pair of interacting orbitals to the total bond energy. Therefore, the EDA–NOCV scheme provides not only qualitative but also quantitative information about the relative strengths of the most significant orbital interactions between the interacting species along the reaction coordinate.

3. Dihydrogen activation and hydrogenation reactions mediated by intramolecular FLPs

(a) Dihydrogen activation reaction

We first focused on the activation of H_2 and the subsequent hydrogenation reaction of unsaturated organic substrates. To this end, we considered the H_2-activation reaction mediated by a particular type of intramolecular FLPs, namely the geminal aminoboranes ($R'_2N–CH_2–BR_2$, **1**) depicted in Fig. 1,[19] which strongly resemble related geminal B/N and B/P FLPs studied experimentally.[20,21]

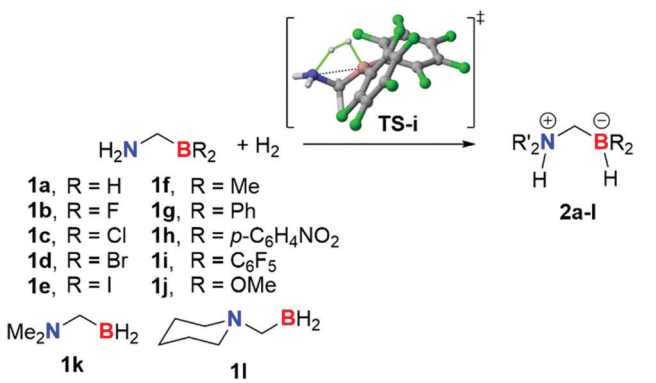

Fig. 1 H_2-activation reactions mediated by $R'_2N–CH_2–BR_2$ FLPs (**1**).

In all cases, the H_2-activation reaction is confirmed to occur concertedly through a five-membered transition state (**TS**, see Fig. 1 for a representative case involving **1i**) which leads to the formation of the corresponding zwitterionic product **2**. Not surprisingly, it is found that good electron-withdrawing groups or soft π-donor substituents at the boron atom of the FLP lead to significantly lower barriers than those processes involving good π-donor groups. For instance, whereas a high free activation barrier of 40.5 kcal mol^{-1} was computed for the process involving **1j** (R = OMe), a much lower barrier of 18.6 kcal mol^{-1} was computed for the analogous reaction mediated by **1i** (M06-2X/def2-TZVPP level), which bears the strong electron-withdrawing group C_6F_5. In addition, it is found that lower barrier processes are associated with both more exothermic reactions and earlier transition states. Indeed, a very good linear correlation was found when plotting the computed reaction energies *versus* the key H···H bond-breaking distances in the corresponding transition states (Fig. 2, correlation coefficient of 0.97), which therefore indicates that these FLP-mediated H_2 activation reactions fulfil the Hammond–Leffer postulate.[22]

The Activation Strain Model (ASM) method was applied then to understand, in a quantitative manner, the above reactivity trends and the origin of the reaction barriers in these FLP-promoted dihydrogen activation reactions. Fig. 3 shows the Activation Strain Diagrams (ASDs) computed for the extreme situations represented by the processes involving **1i** (R = C_6F_5) and **1j** (R =OMe), from the initial reactant complexes to the corresponding transition states and projected onto the N···H bond-forming distance (therefore, the last point in this plot and subsequent figures herein correspond to the respective transition states). From the data in Fig. 3, it becomes clear that the strain energy, *i.e.* the energy penalty associated with the deformation of the reactants required to adopt the TS-geometry, is not at all responsible for the lower barrier computed for the reaction involving **1i** as the ΔE_{strain} term is less destabilizing for

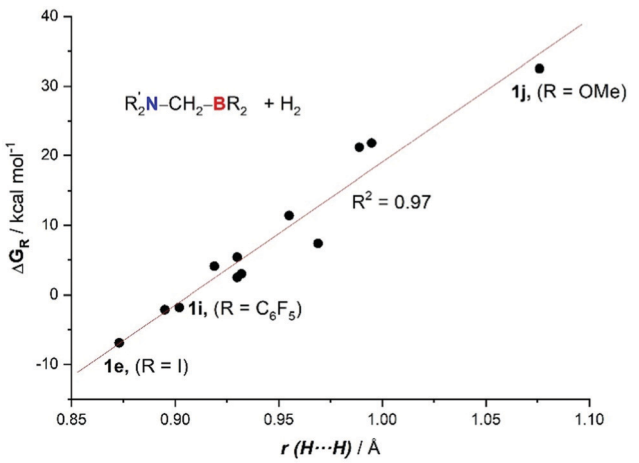

Fig. 2 Plot of the free reaction barriers (ΔG_R) *vs.* the H···H bond distances in the corresponding **TSs** computed for the H_2-activation reactions mediated by geminal FLPs **1**.

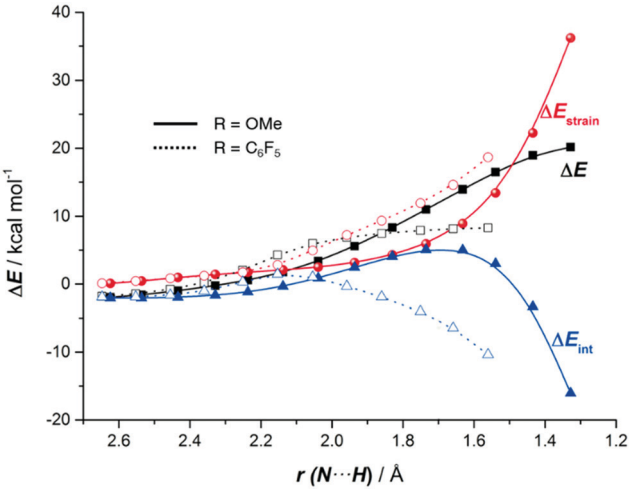

Fig. 3 Comparative activation-strain diagrams of the H_2 activation reactions mediated by geminal FLPs **2j** (R = OMe, solid lines) and **2i** (R = C_6F_5, dashed lines), along the reaction coordinate projected onto the forming N···H bond distance. All data have been computed at the M06-2X/def2-TZVPP level.

the H_2-activation reaction mediated by **1j**. At variance, the lower barrier of the process involving **1i** finds its origin exclusively in the much stronger interaction energy (measured by the ΔE_{int} term) between the deformed reactants, particularly at the transition state region. Therefore, it is found that electron-withdrawing groups directly attached to the acidic center allow a more effective (*i.e.* more stabilizing) interaction between the FLP and H_2 molecules along the entire transformation than that provided by π-donor groups.

The Energy Decomposition Analysis (EDA) method allows us to further decompose the crucial ΔE_{int} term into different chemically meaningful terms (see above). As shown in Fig. 4, which graphically depicts the evolution of the EDA terms along the reaction coordinate once again from the early stages of the processes involving **1i** and **1j** to the corresponding transition states, it becomes evident that the stronger interaction computed for the process involving **1i** derives mainly from stronger orbital interactions (ΔE_{orb} term) and also stronger electrostatic attractions (albeit to a lesser extent, ΔV_{elstat}) between the deformed reactants practically along the entire reaction coordinate. These stabilizing interactions can offset the more destabilizing effect of the ΔE_{Pauli} term computed for the activation reaction mediated by this particular geminal FLP.

The Natural Orbital for Chemical Valence (NOCV) extension of the EDA method was applied next to not only identify but also quantify the main molecular orbital contributions to the crucial ΔE_{orb} term. Fig. 5 shows snapshots of the main NOCV deformation densities dominating the ΔE_{orb} term at three key points along the reaction coordinate (*i.e.* initial reactant complex, midpoint, and TS) for the reaction mediated by **1i**. As depicted in Fig. 5, at the beginning of the transformation, the principal charge depletion region (in red) belongs to the H–H σ-orbital whereas the charge accumulation (in blue) corresponds to the empty p_z atomic orbital at the boron center

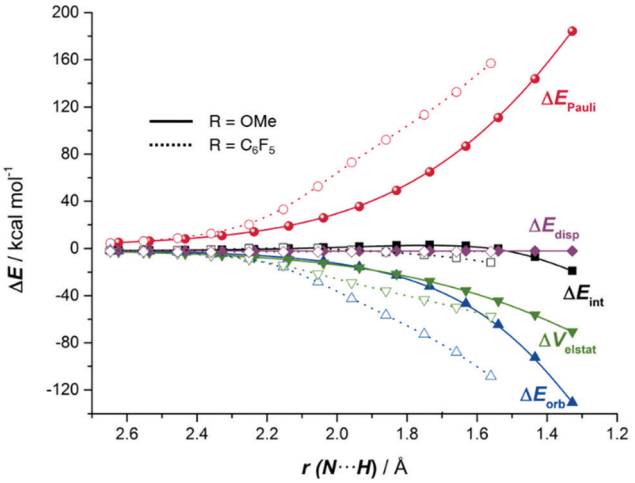

Fig. 4 Comparative energy decomposition analyses of the H_2 activation reactions mediated by geminal FLPs **2j** (R = OMe, solid lines) and **2i** (R = C_6F_5, dashed lines), along the reaction coordinate projected onto the forming N···H bond distance. All data have been computed at the ZORA-BP86-D3/TZ2P//M06-2X/def2-TZVPP level.

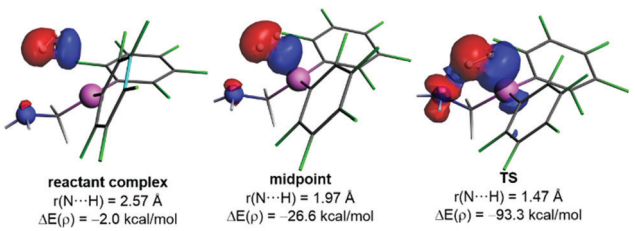

Fig. 5 Contour plots of NOCV deformation densities $\Delta\rho$ and associated energies $\Delta E(\rho)$ (in kcal mol^{-1}) for the main orbital interactions involved in the H_2 activation reaction mediated by geminal FLP **2i** at different stages of the transformation. Electronic charge flows from red to blue. All data were computed at the ZORA-BP86-D3/TZ2P//M06-2X/def2-TZVPP level.

(*i.e.* $\sigma(H_2)\rightarrow p_z(B)$ interaction). As the transformation progresses, this charge transfer continuously reinforces and dominates up to the transition state region. Interestingly, the cooperative charge flow involving the $LP(N)\rightarrow\sigma^*(H_2)$ interaction starts to appear at the midpoint and it is fully developed at the transition state. Therefore, although this NOCV analysis is in line with the Pápai's ET mechanism commented in the introduction,[8] it differs in that both orbital interactions do not take place simultaneously but at rather different stages of the transformation. Thus, the EDA–NOCV identifies that the $\sigma(H_2)\rightarrow p_z(B)$ interaction solely occurs at the very beginning of the process and is responsible for the polarization of the H–H σ-bond, which allows the ulterior interaction with the LP(N) orbital. Similar NOCV deformation densities were found for the higher barrier process involving **1j**, but at variance, the associated stabilization energies ($\Delta E(\rho)$) are markedly lower than those computed for the analogous reaction involving **1i** (Fig. 5), which is then translated into lower ΔE_{orb} and ΔE_{int} values and ultimately, into a higher activation barrier.

(b) Hydrogenation reactions of unsaturated organic compounds

Once the H_2-activation reaction was studied, we then focused on the subsequent hydrogenation reactions of simple unsaturated organic compounds, either polar systems (such as formaldehyde, acetone or methanimine) or apolar substrates (ethylene or acetylene), promoted by the readily formed zwitterionic species **2** (Fig. 6).[23]

Our calculations indicate that in all cases the H_2 release from compounds **2** proceeds in a concerted manner through a seven-membered transition state (see Fig. 6 for the transition state involved in the reaction **2i** + $H_2C{=}NH$). When polar substrates are involved, the process involves the asynchronous nucleophilic attack of the B–H hydride species onto the electrophilic C=X carbon atom of the substrate and the N–H proton migration onto the heteroatom X. For apolar substrates, the process is rather similar yet much more synchronous. Therefore, the transformation can be formally viewed as a double group transfer reaction (DGTR),[24] thus resembling textbook reactions such as the diimide reduction of C=C or C≡C bonds,[25] the Meerwein–Ponndorf–Verley reduction (MPV) of carbonyl groups,[26] and related type II dyotropic reactions.[27]

Moreover, it is found that the hydrogenation of polar multiple bonds (C=O, C=N) is much easier, from a kinetic point of view, than that involving nonpolar bonds (C=C, C≡C). This is mainly due to the occurrence of an initial hydrogen bond between the NH moiety of the zwitterion **2** and the heteroatom of the substrate, which significantly increases the interaction between the reactants, not only at the beginning of the process but also along the entire reaction coordinate. Such noncovalent interaction is not present in the reaction involving nonpolar bonds, and as a result, the interaction between the reactants is markedly reduced, which is translated into a much higher activation barrier. This is nicely supported by the ASM method. As depicted in Fig. 7, the ASDs computed for the hydrogenation reactions of methanimine and ethylene promoted by zwitterion **2b** (R = F), from the initial reactant complexes up to the corresponding transition states and projected onto the forming BH···C bond, confirmed that the interaction between the deformed reactants is much stronger (*i.e.* much more stabilizing) for the process involving the polar substrate. In addition, the occurrence of the NH···N hydrogen bond also leads to a significant reduction of the destabilizing ΔE_{strain}, as a consequence of the closer proximity of the reactive centers.

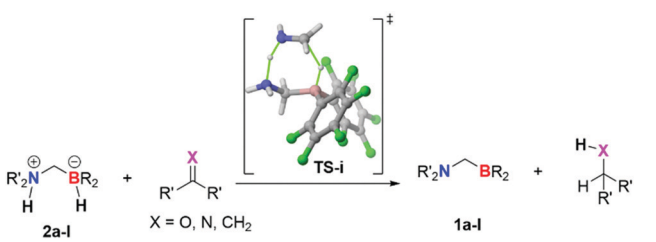

Fig. 6 Hydrogenation reactions of unsaturated organic compounds promoted by zwitterionic species **2**.

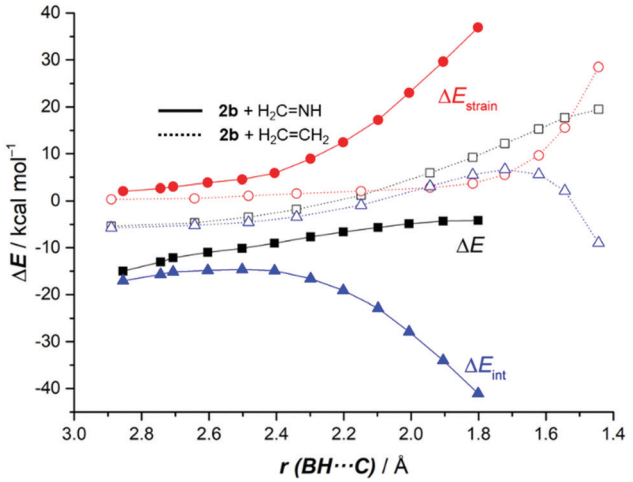

Fig. 7 Comparative activation-strain diagrams of the hydrogenation reactions of methanimine (solid lines) and ethylene (dashed lines) mediated by zwitterion **2b** (R = F) along the reaction coordinate projected onto the forming BH···C bond distance. All data have been computed at the M06-2X/def2-TZVPP level.

Due to the resemblance of this hydrogenation process with related pericyclic DGTRs, it is not surprising that the EDA method identifies the orbital interaction (ΔE_{orb}) as the main contributor to the total interaction energy. Closer inspection of the deformation densities computed by the NOCV method suggests that two main orbital interactions are present in the hydrogenation reaction, namely the LP(heteroatom)→σ*(N–H) interaction (denoted as ρ_1) and the σ(B–H)→π*(X=CH_2) interaction (denoted as ρ_2, Fig. 8). Interestingly, while the former interaction dominates at the early stages of the transformation, the latter becomes the major contributor to the total ΔE_{orb} term in the transition state region (see Fig. 8), which indicates that the NH···X interaction induces a significant polarization of the

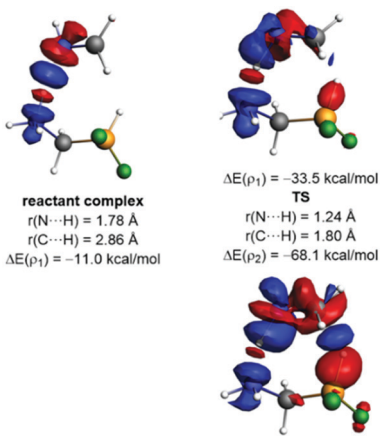

Fig. 8 Contour plots of NOCV deformation densities $\Delta\rho$ and associated energies $\Delta E(\rho)$ (in kcal mol^{-1}) for the main orbital interactions involved in the hydrogenation reaction of methanimine promoted by zwitterion **2b** (R = F) at different stages of the transformation. Electronic charge flows from red to blue. All data were computed at the ZORA-BP86-D3/TZ2P//M06-2X/def2-TZVPP level.

C=X bond which facilitates the subsequent B(H) hydride transfer.

4. Influence of the nature of the LB/LA on the reactivity: rational design of highly active FLPs

(a) Influence of group 13/group 15 elements

Results above suggest that the reactivity of the FLPs can be effectively tuned by modifying the nature of the substituents directly attached to the boron center, which in turn control the acidity of the LA partner. With this in mind, we performed an extensive study on the influence of the nature of both the LB and the LA partners on the reactivity of geminal FLPs of the type $Me_2E–CH_2–E'Ph_2$ (E = group 15 element, E′ = group 13 element),[28] which are strongly related to the $^tBu_2P–CH_2–BPh_2$ FLP experimentally described by Lammertsma and co-workers.[21b]

Once again, we focused on the parent dihydrogen activation reaction which, in all cases, is confirmed to proceed in a concerted manner leading to the corresponding zwitterionic products analogous to **2** through the respective five-membered transition states **TS**. Two main reactivity trends emerged from the computed activation barriers: on one hand, the barrier increases when going down in the group 15 for a given group 13 E′ atom (*i.e.* $\Delta E^{\neq}$ increases in the order E = N < P < As <Sb), and on the other hand, for a given group 15 atom E, the barrier decreases when going down in the group 13, with the notable exception of E′ = Al, which presents systematically the lowest activation barriers in all series. Therefore, our calculations identify the geminal $Me_2N–CH_2–AlPh_2$ FLP as the most active system for the dihydrogen activation reaction.

According to the ASM, the reduced reactivity of the FLP containing heavier group 15 elements finds its origin exclusively in a more destabilizing strain energy (ΔE_{strain}) as compared to the lighter N-FLP (Fig. 9). The interaction energy (ΔE_{int}) is however rather similar for all systems, and hence it is not all responsible for the observed reactivity trend. Therefore, our calculations suggest that the equilibrium geometry of the N-FLP better fits into the corresponding transition state geometry, and consequently, requires a lower distortion energy than its heavier counterparts.

The ASM was also helpful to understand the trend observed when varying the nature of the group 13 element. As shown in Fig. 10, the heavier systems (E′ = Al, In) benefit from a less destabilizing strain energy together with a stronger interaction between the deformed reactants along the entire reaction coordinate as compared to their B-analogue. The ASDs depicted in Fig. 10 also explain the peculiar behaviour of the Al-FLP, which, as commented above, exhibits the lowest barriers in all the series. As clearly seen, while the reaction involving this particular FLP exhibits a rather similar ΔE_{strain} as its heavier In-analogue, it benefits from a significantly stronger interaction, particularly at the transition state region. This is, according to the EDA–NOCV method, exclusively ascribed to a higher

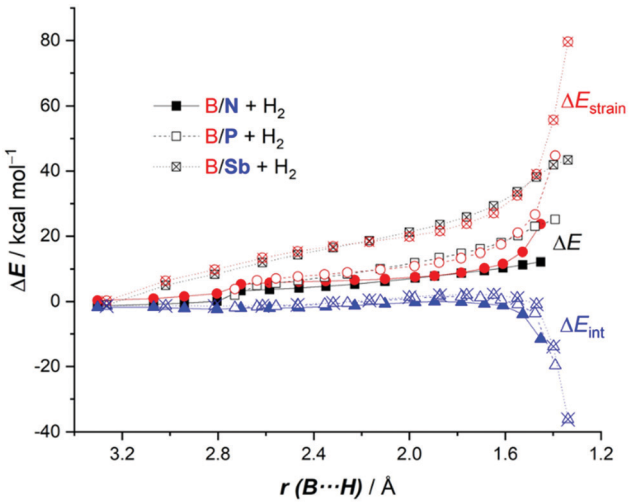

Fig. 9 Comparative activation-strain diagrams of the H_2 activation reactions mediated by geminal $Me_2E–CH_2–BPh_2$ FLPs (E = N, solid lines; E = P, dashed lines; E = Sb, dotted lines) along the reaction coordinate projected onto the forming B···H bond distance. All data have been computed at the M06-2X/def2-TZVPP level.

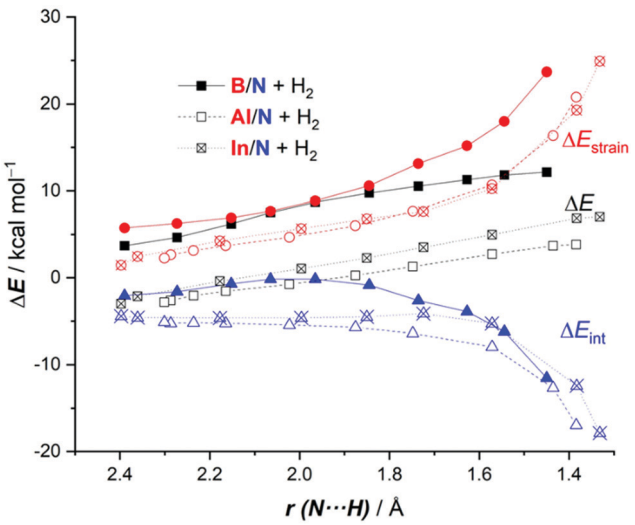

Fig. 10 Comparative activation-strain diagrams of the H_2 activation reactions mediated by geminal $Me_2N–CH_2–E'Ph_2$ FLPs (E′ = B, solid lines; E′ = Al, dashed lines; E′ = In, dotted lines) along the reaction coordinate projected onto the forming B···H bond distance. All data have been computed at the M06-2X/def2-TZVPP level.

cooperative $\sigma(H_2)\rightarrow p_z(E')/LP(N)\rightarrow\sigma^*(H_2)$ molecular orbital interactions (for instance, as the same consistent N···H bond-forming distance of 1.5 Å, the corresponding stabilizing energy, $\Delta E(\rho)$, is *ca.* 8 kcal mol^{-1} higher for the process mediated by the Al-FLP than that mediated by the In-FLP).

Our computational screening therefore identifies the geminal FLPs composed of N/B and, particularly, N/Al as the most active species for the activation of dihydrogen. To further enhance the reactivity of these FLPs and based on the

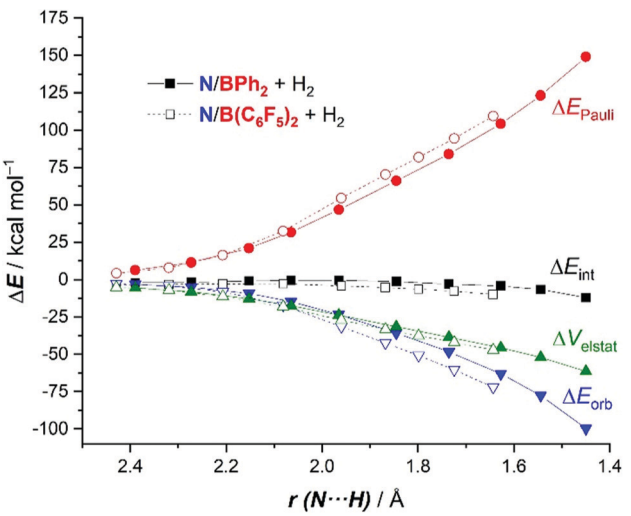

Fig. 11 Comparative energy decomposition analyses of the of the H_2 activation reactions mediated by geminal FLPs $Me_2N–CH_2–B'R_2$ (R = Ph, solid lines; R = C_6F_5, dashed lines), along the reaction coordinate projected onto the forming N···H bond distance. All data have been computed at the ZORA-M06-2X/TZ2P//M06-2X/def2-TZVPP level.

substituent effects found in the previous chapter,[19] we increased the acidity of the LA partner by attaching strong electron-withdrawing groups to the group 13 element. Not surprisingly, the replacement of the phenyl groups in $Me_2N–CH_2–E'Ph_2$ (E′ = B, Al) by the highly acceptor C_6F_5 or Fxyl (Fxyl = 3,5-$(CF_3)_2C_6H_3$)[29] groups leads to a significant enhancement of the reactivity of the corresponding FLPs as viewed from the remarkable reduction of the respective activation barriers (up to *ca.* 10 kcal mol^{-1}). According to the ASM method, this reduction in the barrier is due to the combination of an increased interaction between the deformed reactants and also to a significant reduction of the destabilizing deformation energy.[28] The corresponding EDA diagrams (Fig. 11) ascribed the enhanced interaction in the C_6F_5-substituted system mainly to stronger orbital interactions (mainly the key $\sigma(H_2)\rightarrow p_z(B)$ interaction) and, to a lesser extent, to stronger electrostatic interactions.

The insight gained by the application of the ASM–EDA (NOCV) method allowed us to further design highly active geminal FLPs. We hypothesised that the introduction of the highly acidic, 4π-antiaromatic borole[30] fragment as the LA would significantly enhance the reactivity of the geminal FLP.[31] In this sense, the gain in aromaticity in the borole moiety during the activation of a small molecule (not only H_2 but also CO_2, CS_2, HC≡CH, SiH_4 and even CH_4) should result in a gain of stability in both the corresponding transition state, therefore leading to a lower barrier transformation, and in the final zwitterionic adduct, therefore making the process thermodynamically more favourable. Our calculations clearly supported this hypothesis and, as depicted in Fig. 12 for the activation of H_2, the borole substituted FLP **4** is much more reactive than the already highly active parent FLP **3** described by Lammertsma and co-workers.[21b] Therefore, and

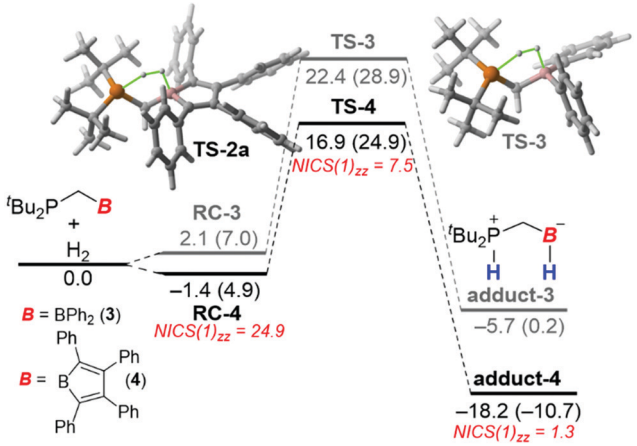

Fig. 12 Comparative computed reaction profiles for the dihydrogen activation mediated by FLPs **3** and **4**. Relative energies (free energies within parentheses) are given in kcal mol^{-1}. All data have been computed at the PCM(toluene)-M06-2X/def2-TZVPP//M06-2X/def2-SVP level.

as supported by Nuclear Independent Chemical Shift (NICS)[32] calculations and the Anisotropy of the Induced Current Density (ACID)[33] method, it is confirmed that aromaticity can be also a key factor to control the reactivity of FLPs. This is further confirmed by the results involving the FLP having a 2π-aromatic borirene in its structure, which, in sharp contrast, is much less reactive than the parent system **3**.[31]

(b) FLPs containing group 14 elements as LA partners

As commented in the introduction, the number of FLPs described so far in the literature is impressive. Although the vast majority of the systems are based on group 13/group 15 combinations, many other different systems have been prepared to tune their properties and reactivity. In this sense, Mitzel and co-workers have recently prepared a series of group 14 element containing neutral geminal FLPs, *i.e.*, $(F_5C_2)_3E–CH_2–P(^tBu)_2$, E = Si,[34] Ge,[35] Sn,[36] which have been proven to readily activate small molecules such as CO_2, SO_2, CS_2, HCl, or phenyl isocyanate (Fig. 13), therefore resembling the reactivity of more traditional B/P FLPs. Despite this resemblance, very little was known about the actual influence of the nature of the group 14 element on the reactivity of these novel geminal FLPs. This encouraged us to carry out a comparative study on the reactivity of the above group 14 element containing FLPs against CO_2 and phenyl isocyanate including the parent P/B system $Ph_2B–CH_2–P(^tBu)_2$ (**3**).[37]

Our calculations indicate that both processes also occur in a concerted manner through a five-membered transition state which leads to the corresponding zwitterionic reaction product (see Fig. 13). It is found that the reactivity of these systems increases when going down in the group 14 (*i.e.* the barrier height $\Delta E^{\neq}$ decreases in the order E = Si > Ge > Sn), which is in nice agreement with the experimental observations.[34–36] Interestingly, the computed barriers are comparable and even lower (when E = Ge, Sn) than that computed for the reactions mediated by the parent P/B-FLP **3**.

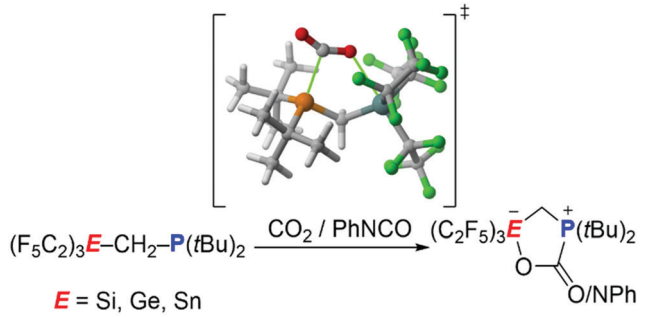

Fig. 13 CO_2 and PhNCO activation reactions promoted by group 14 containing FLPs reported by Mitzel and co-workers (see ref. 34–36).

To understand the reasons behind this reactivity trend we applied the ASM method. Fig. 14 shows the computed ASDs for the $(F_5C_2)_3E–CH_2–P(^tBu)_2$ + PhNCO reactions from the initial reactant complexes up to the respective transition states and projected onto the P···C bond-forming distance. From the data in Fig. 14, it becomes evident that the heavier systems benefit from both a less destabilizing strain energy and a stronger interaction between the reactants along the entire reaction coordinate as compared to the lighter system (E = Si). The more stabilizing interaction computed for the processes involving E = Ge, Sn derives, according to the EDA method, from both stronger electrostatic and orbital attractions in a nearly identical extent.[37]

Finally, the NOCV extension of the EDA was key to identify (and also quantify) the main orbital interactions involved in these activation reactions promoted by these FLPs prepared by Mitzel and co-workers. Thus, at the very beginning of the process, the donation of electron density from the lone pair

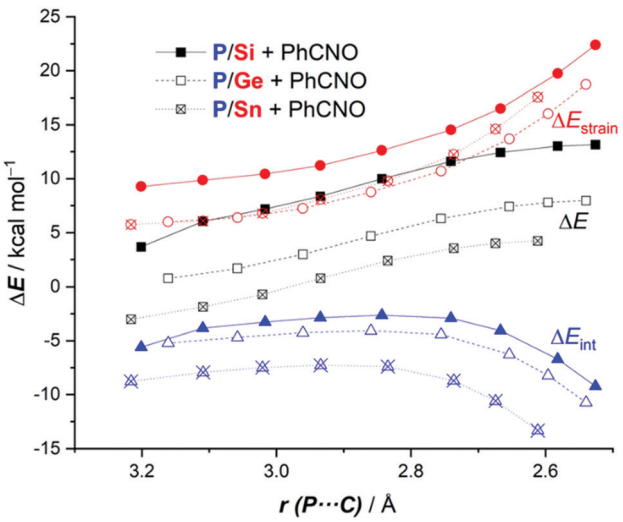

Fig. 14 Comparative activation-strain diagrams of the phenyl isocyanate activation reactions mediated by geminal $(F_5C_2)_3E–CH_2–P(^tBu)_2$ FLPs (E = Si, solid lines; E = Ge, dashed lines and E = Sn, dotted lines) along the reaction coordinate projected onto the forming P···C bond distance. All data have been computed at the PCM(toluene)-M06-2X/def2-TZVPP//M06-2X/def2-SVP level.

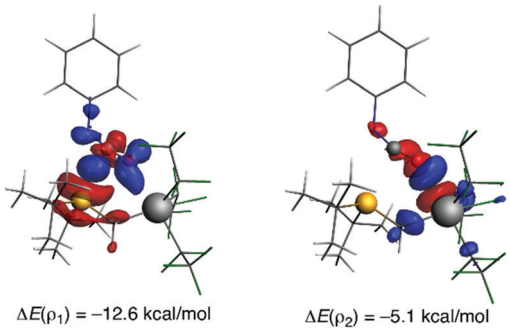

Fig. 15 Contour plots of NOCV deformation densities $\Delta\rho$ and associated energies $\Delta E(\rho)$ (in kcal mol^{-1}) for the main orbital interactions between PhNCO and geminal FLP $(F_5C_2)_3Sn{-}CH_2{-}P(tBu)_2$ FLPs computed at a P···C forming bond distance of 2.7 Å. Electronic charge flows from red to blue. All data were computed at the ZORA-M06-2X/TZ2P//M06-2X/def2-SVP level.

of the phosphorus atom of the FLP to the LUMO of the phenyl isocyanate, *i.e.* LP(P) $\rightarrow\pi^*$(C═O) interaction (denoted as ρ_1, see Fig. 15), dominates. As the reaction progresses, this orbital interaction reinforces up to the transition state region, where the donation from the negatively charged oxygen atom of the isocyanate to the $E(C_2F_5)_3$ moiety, *i.e.* LP(O)$\rightarrow\sigma^*$(E–C) interaction (denoted as ρ_2), starts to take place. This collaborative yet asynchronous electron density flow therefore resembles that found for the H_2-activation reactions promoted by group 13/group 15-FLPs commented above, thus suggesting a general mode of reactivity for geminal FLPs, regardless of the nature of the LA/LB antagonists.

5. Reactivity of intermolecular FLPs: the case of carbones and heavier ylidones as LBs

The applicability of the ASM–EDA(NOCV) approach to quantitatively understanding the reactivity of FLPs is not restricted to intramolecular systems similar to the geminal species described above. On the contrary, it can be successfully applied to intermolecular systems as well.[38,39] As a representative example, we became intrigued by the report by Alcarazo and co-workers on the use of the parent carbone, $C(PPh_3)_2$, as LB in FLP chemistry.[40] Indeed, this species, where the central carbon atom retains all four valence electrons as two lone pairs,[41] in combination with the $B(C_6F_5)_3$ LA form a highly active FLP which is able to activate not only H–H bonds but also C–O, C–H, Si–H, and C–F bonds (Fig. 16). This report offered us then a paramount opportunity to (i) compare the effect of the replacement of typical LBs such as phosphines by carbones on the reactivity of intermolecular FLPs and (ii) investigate the possible use of heavier ylidones (EL_2, E = group 14 element, L = phosphine, *N*-heterocyclic carbene) as LBs.[39]

We first focused on the H_2-activation reaction promoted by the parent intermolecular system $^tBu_3P/B(C_6F_5)_3$, used initially by Stephan and co-workers,[42] and the analogous reaction

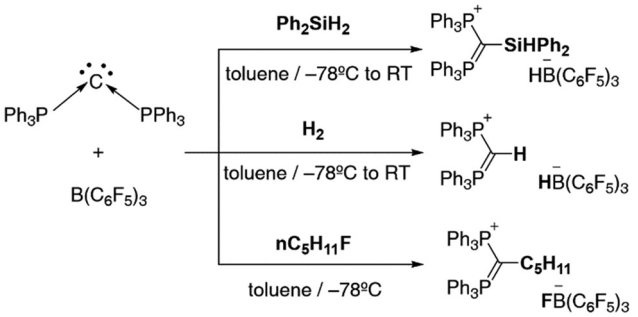

Fig. 16 Reactivity of carbone $C(PPh_3)_2$ as LB in FLP chemistry reported by Alcarazo and co-workers (see ref. 40).

involving the $(Me_3P)_2C/B(C_6F_5)_3$ pair. In both cases, it is found that the heterolytic H_2 splitting occurs in a concerted manner through the formation of an initial reactant complex which evolves into the corresponding reaction product in a strongly exothermic process.[39] Despite that, the process involving the carbone as LB is favoured along the entire reaction coordinate, and particularly in the reaction product region, over the analogous reaction involving the phosphine, which is consistent with the experimental observations. According to the EDA method, the computed total interaction energy between the [LB···LA] and H_2 reactants become rather similar for both reactions (Fig. 17). Despite that, there exist significant differences in the mode of action of the $(Me_3P)_2C/B(C_6F_5)_3$ and $^tBu_3P/B(C_6F_5)_3$ pairs. As shown in Fig. 17, the carbone system benefits from both stronger electrostatic and orbital attractions along the entire reaction coordinate as compared to the phosphine-based FLP.

When applying the NOCV method, the differences between both intermolecular FLPs become even more evident. In both

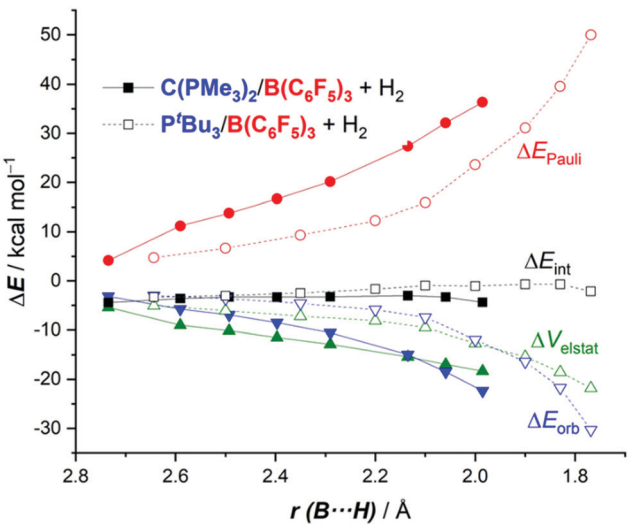

Fig. 17 Comparative energy decomposition analyses of the H_2 activation reactions mediated by $C(PMe_3)_2$ (solid lines) and $^tBu_3P$ (dashed lines) in the presence of $B(C_6F_5)_3$ along the reaction coordinate projected onto the forming B···H bond length. All data were computed at the M06-2X/TZ2P//M06-2X/def2-SVP level.

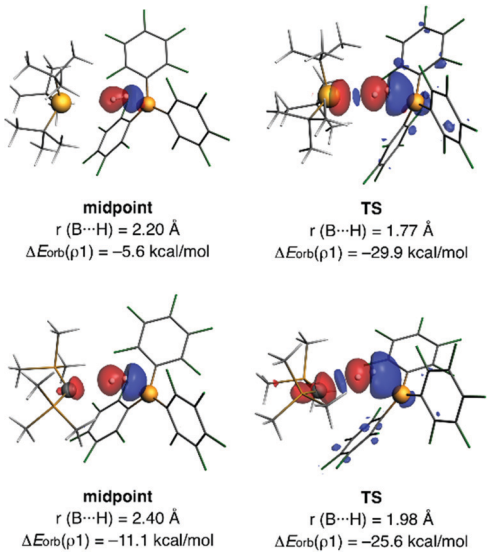

Fig. 18 Contour plots of NOCV deformation densities $\Delta\rho$ and associated energies $\Delta E(\rho)$ (in kcal mol^{-1}) for the main orbital interactions between H_2 and [^{t}Bu$_3$P···B(C$_6$F$_5$)$_3$] (top) and [C(PMe$_3$)$_2$···B(C$_6$F$_5$)$_3$] (bottom). Electronic charge flows from red to blue. All data were computed at the M06-2X/TZ2P//M06-2X/def2-SVP level.

cases, the $\sigma(H_2)\rightarrow p_z(B)$ interaction is the dominant orbital from the beginning of the process up to the transition state region, where the LP(P/C)$\rightarrow\sigma^*(H_2)$ interaction takes place (Fig. 18). This mode of action then strongly resembles the cooperative, asynchronous mode described above for intramolecular systems. Despite that, in the process involving the carbone as LB, the associated orbital energies are comparatively higher along the entire process. This is a consequence of the involvement of the LP(C)$\rightarrow\sigma^*(H_2)$ interaction also from the very beginning of the process (see Fig. 18, midpoint) as a consequence of the well-known higher σ-donor ability of C(PMe$_3$)$_2$ as compared to ^{t}Bu$_3$P.

We finally also explored the influence on the reactivity of the nature of both the central E atom (E = C–Pb) as well as the surrounding ligands L (L = phosphine *vs.* carbene) in EL$_2$ compounds as LBs. It was found that heavier ylidones become more reactive than the parent carbones CL$_2$ as confirmed by the decrease of the computed barrier heights of the corresponding H_2 activation reactions upon moving down group 14 ($\Delta E^{\neq}$ reduction up to *ca.* 8 kcal mol^{-1}). This enhanced reactivity of heavier ylidones is ascribed by the ASM–EDA(NOCV) method to a stronger interaction between the deformed reactants, which derives from more stabilizing orbital interactions (mainly the key LP(E)$\rightarrow\sigma^*(H_2)$ interaction).[39] Therefore, our calculations predict that heavier ylidones are promising candidates to act as LBs in FLPs to achieve facile H_2-activation reactions.

6. Summary and outlook

In this Feature article, we have highlighted our recent results on the application of the ASM–EDA(NOCV) method to gain a more detailed and quantitative insight into the reactivity of Frustrated Lewis Pairs. Through representative examples, we have proposed a mode of small molecule activation which involves the cooperative action of the LB and LA, *i.e.* the key $\sigma(H_2)\rightarrow p_z(LA)$ and LP(LB)$\rightarrow\sigma^*(H_2)$ molecular orbital interactions, occurring at rather different stages of the transformation. In this sense, our approach nicely complements the existing reactivity models in the literature, particularly the Pápai's ET model. In addition, the insight gained by the ASM–EDA(NOCV) method allowed us to rationally design highly active FLPs to achieve facile small molecule activation reactions. Thus, intramolecular geminal systems based on N/B and N/Al combinations where the LA partner is decorated with highly electron-withdrawing groups, and particularly borole groups, and intermolecular systems involving heavy ylidones as LBs are really promising candidates to be tested experimentally.

We strongly believe that the results summarized herein firmly confirm that the ASM–EDA(NOCV) approach is a powerful tool to not only rationalize the reactivity of FLPs but also to get a detailed insight into the so far not fully understood cooperative mode of action of the LB/LA partners. In our opinion, the ASM–EDA(NOCV) methodology can be a really useful tool to guide experimentalists towards the rational development of novel, highly active FLP systems.

Conflicts of interest

There are no conflicts to declare.

Acknowledgements

This work was supported by the Spanish MCIN/AEI/10.13039/501100011033 (Grants PID2019-106184GB-I00 and RED2018-102387-T).

Notes and references

1 For leading reviews, see: (*a*) D. W. Stephan and G. Erker, *Angew. Chem., Int. Ed.*, 2010, **49**, 46; (*b*) G. Erker, *Pure Appl. Chem.*, 2012, **84**, 2203; (*c*) D. W. Stephan and G. Erker, Top. Curr. Chem., *Frustrated Lewis Pairs I*, Springer, Heidelberg, vol. 332, 2013; (*d*) D. W. Stephan and G. Erker, *Chem. Sci.*, 2014, **5**, 2625; (*e*) D. W. Stephan, *J. Am. Chem. Soc.*, 2015, **137**, 10018; (*f*) D. W. Stephan and G. Erker, *Angew. Chem., Int. Ed.*, 2015, **54**, 6400; (*g*) D. W. Stephan, *Acc. Chem. Res.*, 2015, **48**, 306; (*h*) D. W. Stephan, *Science*, 2016, **354**, aaf7229.
2 (*a*) D. W. Stephan, *Chem*, 2020, **6**, 1520; (*b*) A. R. Jupp and D. W. Stephan, *Trends Chem.*, 2019, **1**, 35.
3 G. C. Welch, R. R. San Juan, J. D. Masuda and D. W. Stephan, *Science*, 2006, **314**, 1124.
4 (*a*) J. Lam, K. M. Szkop, E. Mosaferi and D. W. Stephan, *Chem. Soc. Rev.*, 2019, **48**, 3592; (*b*) W. Meng, X. Feng and H. Du, *Acc. Chem. Res.*, 2018, **51**, 191; (*c*) D. W. Stephan, *J. Am. Chem. Soc.*, 2021, **143**, 20002.
5 M. Hong, J. Chen and E. Y. Chen, *Chem. Rev.*, 2018, **118**, 10551.
6 (*a*) K. K. Ghuman, T. E. Wood, L. B. Hoch, C. A. Mims, G. A. Ozin and C. V. Singh, *Phys. Chem. Chem. Phys.*, 2015, **17**, 14623; (*b*) Z. Niu, W. D. C. Bhagya Gunatilleke, Q. Sun, P. C. Lan, J. Perman, J.-G. Ma, Y. Cheng, B. Aguila and S. Ma, *Chem*, 2018, **4**, 2587.
7 (*a*) S. Arndt, M. Rudolph and A. S. K. Hashmi, *Gold Bull.*, 2017, **50**, 267; (*b*) J. Campos, *J. Am. Chem. Soc.*, 2017, **139**, 2944; (*c*) N. Hidalgo, J. J. Moreno, M. Pérez-Jiménez, C. Maya, J. López-Serrano and J. Campos, *Chem. – Eur. J.*, 2020, **26**, 5982; (*d*) N. Hidalgo, J. J. Moreno,

M. Pérez-Jiménez, C. Maya, J. López-Serrano and J. Campos, *Organometallics*, 2020, **39**, 2534.
8 (*a*) T. A. Rokob, A. Hamza, A. Stirling, T. Soós and I. Pápai, *Angew. Chem., Int. Ed.*, 2008, **47**, 2435; (*b*) T. A. Rokob, A. Hamza and I. Pápai, *J. Am. Chem. Soc.*, 2009, **131**, 10701; (*c*) T. A. Rokob, I. Bakj, A. Stirling, A. Hamza and I. Pápai, *J. Am. Chem. Soc.*, 2013, **135**, 4425.
9 (*a*) S. Grimme, H. Kruse, L. Goerigk and G. Erker, *Angew. Chem., Int. Ed.*, 2010, **49**, 1402; (*b*) B. Schirmer and S. Grimme, *Chem. Commun.*, 2010, **46**, 7942.
10 L. Rocchigiani, G. Ciancaleoni, C. Zuccaccia and A. Macchioni, *J. Am. Chem. Soc.*, 2014, **136**, 112.
11 (*a*) L. Liu, L. L. Cao, Y. Shao, G. Menard and D. W. Stephan, *Chem*, 2017, **3**, 259; (*b*) F. Holtrop, A. R. Jupp, B. J. Kooij, N. P. Leest, B. de Bruin and J. C. Slootweg, *Angew. Chem., Int. Ed.*, 2020, **59**, 22210; (*c*) F. Holtrop, A. R. Jupp, N. P. Leest, M. P. Domínguez, R. M. Williams, A. M. Brouwer, B. de Bruin, A. W. Ehlers and J. C. Slootweg, *Chem. – Eur. J.*, 2020, **26**, 9005.
12 For reviews, see: (*a*) I. Fernández and F. M. Bickelhaupt, *Chem. Soc. Rev.*, 2014, **43**, 4953; (*b*) F. M. Bickelhaupt and K. N. Houk, *Angew. Chem., Int. Ed.*, 2017, **56**, 10070; (*c*) P. Vermeeren, T. A. Hamlin and F. M. Bickelhaupt, *Chem. Commun.*, 2021, **57**, 5880. See also: (*d*) I. Fernández, in *Discovering the Future of Molecular Sciences*, ed. B. Pignataro, Wiley-VCH, Weinheim, 2014, pp. 165–187.
13 For reviews on the EDA method, see: (*a*) F. M. Bickelhaupt and E. J. Baerends, in *Rev. Comput. Chem.*, ed. K. B. Lipkowitz and D. B. Boyd, Wiley-VCH, New York, 2000, vol. 15, pp. 1–86; (*b*) M. von Hopffgarten and G. Frenking, *Wiley Interdiscip. Rev.: Comput. Mol. Sci.*, 2012, **2**, 43; (*c*) G. Frenking and F. M. Bickelhaupt, in *The Chemical Bond: Fundamental Aspects of Chemical Bonding*, ed.G. Frenking and S. Shaik, Wiley-VCH, Weinheim, 2014, pp. 121–158; (*d*) I. Fernández, in *Applied Theoretical Organic Chemistry*, ed. D. J. Tantillo, World Scientific, New Jersey, 2018, pp. 191–226. For a review of different EDA approaches, see; (*e*) M. J. S. Phipps, T. Fox, C. S. Tautermann and C.-K. Skylaris, *Chem. Soc. Rev.*, 2015, **44**, 3177.
14 Representative examples: (*a*) I. Fernández, F. M. Bickelhaupt and F. P. Cossío, *Chem. – Eur. J.*, 2014, **20**, 10791; (*b*) A. K. Narsaria, T. A. Hamlin, K. Lammertsma and F. M. Bickelhaupt, *Chem. – Eur. J.*, 2019, **25**, 9902; (*c*) T. A. Hamlin, I. Fernández and F. M. Bickelhaupt, *Angew. Chem., Int. Ed.*, 2019, **58**, 8922; (*d*) P. Vermeeren, T. A. Hamlin, I. Fernández and F. M. Bickelhaupt, *Angew. Chem., Int. Ed.*, 2020, **59**, 6201; (*e*) P. Vermeeren, T. A. Hamlin, I. Fernández and F. M. Bickelhaupt, *Chem. Sci.*, 2020, **11**, 8105; (*f*) I. Fernández, *Chem. Sci.*, 2020, **11**, 3769; (*g*) S. Yu, P. Vermeeren, T. A. Hamlin and F. M. Bickelhaupt, *Chem. – Eur. J.*, 2021, **27**, 5683; (*h*) S. Portela, J. J. Cabrera-Trujillo and I. Fernández, *J. Org. Chem.*, 2021, **86**, 5317; (*i*) T. A. Hamlin, F. M. Bickelhaupt and I. Fernández, *Acc. Chem. Res.*, 2021, **54**, 1972.
15 Representative examples in organometallic and main-group chemistry: (*a*) O. Nieto Faza, C. S. López and I. Fernández, *J. Org. Chem.*, 2013, **78**, 5669; (*b*) A. G. Green, P. Liu, C. A. Merlic and K. N. Houk, *J. Am. Chem. Soc.*, 2014, **136**, 4575; (*c*) E. D. Sosa Carrizo, F. M. Bickelhaupt and I. Fernández, *Chem. – Eur. J.*, 2015, **21**, 14362; (*d*) Y. García-Rodeja and I. Fernández, *Organometallics*, 2017, **36**, 460; (*e*) S. Chen, X. Huang, E. Meggers and K. N. Houk, *J. Am. Chem. Soc.*, 2017, **139**, 17902; (*f*) A. Couce-Ríos, A. Lledós, I. Fernández and G. Ujaque, *ACS Catal.*, 2019, **9**, 848; (*g*) T. Sergeieva, T. A. Hamlin, S. Okovytyy, B. Breit and F. M. Bickelhaupt, *Chem. – Eur. J.*, 2020, **26**, 2342; (*h*) J. J. Cabrera-Trujillo and I. Fernández, *Chem. – Eur. J.*, 2020, **26**, 11806; (*i*) J. J. Cabrera-Trujillo and I. Fernández, *Chem. – Eur. J.*, 2021, **27**, 12422; (*j*) I. Cortés, J. J. Cabrera-Trujillo and I. Fernández, *Dalton Trans.*, 2021, **50**, 18036.
16 K. Morokuma, *J. Chem. Phys.*, 1971, **55**, 1236.
17 T. Ziegler and A. Rauk, *Theor. Chim. Acta*, 1977, **46**, 1.
18 (*a*) M. Mitoraj and A. Michalak, *J. Mol. Model.*, 2007, **13**, 347; (*b*) M. P. Mitoraj, A. Michalak and T. Ziegler, *J. Chem. Theory Comput.*, 2009, **5**, 962.
19 D. Yepes, P. Jaque and I. Fernández, *Chem. – Eur. J.*, 2016, **22**, 18801.
20 (*a*) E. Theuergarten, J. Schlösser, D. Schlüns, M. Freytag, C. G. Daniliuc, P. G. Jones and M. Tamm, *Dalton Trans.*, 2012, **41**, 9101; (*b*) É. Dorkó, E. Varga, T. Gáti, T. Holczbauer, I. Pápai, H. Mehdi and T. Soós, *Synlett*, 2014, 1525.
21 (*a*) A. Stute, G. Kehr, R. Fröhlich and G. Erker, *Chem. Commun.*, 2011, **47**, 4288; (*b*) F. Bertini, V. Lyaskoyskyy, B. J. J. Timmer, F. J. J. de Kanter, M. Lutz, A. W. Ehlers, J. C. Slootweg and K. Lammertsma, *J. Am. Chem. Soc.*, 2012, **134**, 201; (*c*) J. Yu, G. Kehr, C. G. Daniliuc, C. Bannwarth, S. Grimme and G. Erker, *Org. Biomol. Chem.*, 2015, **13**, 5783; (*d*) K. Samigullin, I. Georg, M. Bolte, H.-W. Lerner and M. Wagner, *Chem. – Eur. J.*, 2016, **22**, 3478; (*e*) E. R. M. Habraken, L. C. Mens, M. Nieger, M. Lutz, A. W. Ehlers and J. C. Slootweg, *Dalton Trans.*, 2017, **46**, 12284.
22 (*a*) J. E. Leffler, *Science*, 1953, **117**, 340; (*b*) G. S. J. Hammond, *J. Am. Chem. Soc.*, 1955, **77**, 334.
23 D. Yepes, P. Jaque and I. Fernández, *Chem. – Eur. J.*, 2018, **24**, 8833.
24 (*a*) S. Sankararaman, *Pericyclic Reactions—A Textbook: Reactions, Applications and Theory*, Wiley-VCH, Weinheim, 2005, pp. 326–329, and references therein. See also; (*b*) I. Fernández, M. A. Sierra and F. P. Cossío, *J. Org. Chem.*, 2007, **72**, 1488; (*c*) F. Cervantes, A. de Cózar, F. P. Cossío, M. Fernández-Herrera, G. Merino and I. Fernández, *Chem. Commun.*, 2015, **51**, 5302; (*d*) I. Fernández and F. P. Cossío, *J. Comput. Chem.*, 2016, **37**, 1265.
25 (*a*) S. Hünig, H. R. Müller and W. Thier, *Angew. Chem., Int. Ed. Engl.*, 1965, **4**, 271; (*b*) M. Franck-Neumann and C. Dietrich-Buchecker, *Tetrahedron Lett.*, 1980, **21**, 671; (*c*) E. W. Garbisch, Jr., S. M. Schildcrout, D. B. Patterson and C. M. Sprecher, *J. Am. Chem. Soc.*, 1965, **87**, 2932.
26 L. Sominsky, E. Rozental, H. Gottlieb, A. Gedanken and S. Hoz, *J. Org. Chem.*, 2004, **69**, 1492.
27 For a review on dyotropic reactions, see: I. Fernández, F. P. Cossío and M. A. Sierra, *Chem. Rev.*, 2009, **109**, 6687.
28 J. J. Cabrera-Trujillo and I. Fernández, *Chem. – Eur. J.*, 2018, **24**, 17823.
29 The FXyl group has been recently used for the preparation of highly active geminal FLPs. See ref. 21*d*.
30 H. Braunschweig, I. Fernández, G. Frenking and T. Kupfer, *Angew. Chem., Int. Ed.*, 2008, **47**, 1951.
31 J. J. Cabrera-Trujillo and I. Fernández, *Chem. Commun.*, 2019, **55**, 675.
32 Z. Chen, C. S. Wannere, C. Corminboeuf, R. Puchta and P. v. R. Schleyer, *Chem. Rev.*, 2005, **105**, 3842.
33 D. Geuenich, K. Hess, F. Köhler and R. Herges, *Chem. Rev.*, 2005, **105**, 3758.
34 B. Waerder, M. Pieper, L. A. Körte, T. A. Kinder, A. Mix, B. Neumann, H.-G. Stammler and N. W. Mitzel, *Angew. Chem., Int. Ed.*, 2015, **54**, 13416.
35 T. A. Kinder, R. Pior, S. Blomeyer, B. Neumann, H.-G. Stammler and N. W. Mitzel, *Chem. – Eur. J.*, 2019, **25**, 5899.
36 P. Holtkamp, F. Friedrich, E. Stratmann, A. Mix, B. Neumann, H.-G. Stammler and N. W. Mitzel, *Angew. Chem., Int. Ed.*, 2019, **58**, 5114.
37 J. J. Cabrera-Trujillo and I. Fernández, *J. Phys. Chem. A*, 2019, **123**, 10095.
38 J. J. Cabrera-Trujillo and I. Fernández, *Chem. – Eur. J.*, 2021, **27**, 3823.
39 J. J. Cabrera-Trujillo and I. Fernández, *Inorg. Chem.*, 2019, **58**, 7828.
40 M. Alcarazo, C. Gomez, S. Holle and R. Goddard, *Angew. Chem., Int. Ed.*, 2010, **49**, 5788.
41 For recent reviews on carbones and related compounds, see: (*a*) G. Frenking, R. Tonner, S. Klein, N. Takagi, T. Shimizu, A. Krapp, K. K. Pandey and P. Parameswaran, *Chem. Soc. Rev.*, 2014, **43**, 5106; (*b*) G. Frenking, M. Hermann, D. M. Andrada and N. Holzmann, *Chem. Soc. Rev.*, 2016, **45**, 1129; (*c*) L. Zhao, M. Hermann, N. Holzmann and G. Frenking, *Coord. Chem. Rev.*, 2017, **344**, 163.
42 G. C. Welch and D. W. Stephan, *J. Am. Chem. Soc.*, 2007, **129**, 1880.

